PHYSICAL REVIEW A VOLUME 37, NUMBER 11 JUNE 1, 1988

Formation and propagation of streamers in N_2 and N_2-SF_6 mixtures

C. Wu and E. E. Kunhardt
Weber Research Institute, Polytechnic University, Farmingdale, New York 11735

(Received 4 June 1987)

In this paper we present results from a self-consistent two-dimensional numerical simulation of the formation and propagation of streamers in nonattaching (N_2) and attaching (N_2-SF_6 mixture) gases using a one-moment fluid model. A numerical technique has been used which allows the solution of the space-charge equations in the presence of large gradients and dynamic range. Photoionization in the gas and photoelectric effect at the cathode have been taken into account. Streamers in the N_2-SF_6 mixture have been found to be considerably different from those in N_2. Spatial oscillations in the electron density have been observed for the N_2-SF_6 mixture, which lead to a more complex field distribution and particle-flow dynamics. The results obtained for N_2 have been compared to those obtained with use of a kinetic description of the electron dynamics. Comparisons with experimental observations and interpretation of experimental observations have been made for both N_2 and N_2-SF_6 mixtures.

I. INTRODUCTION

A considerable amount of theoretical, numerical, and experimental efforts has been devoted to the understanding of the development of an electron avalanche, its transition into streamers, and the propagation of the streamer fronts (see reviews by Kunhardt[1] and Lozanskii[2]). Recent advances in diagnostic and numerical techniques have provided significant new insight into the collective processes that play a major role in the formation and propagation of streamers.[1]

Although kinetic models have been used,[3,4] the vast majority of the numerical simulations of this phenomenon have used fluid equations to describe the evolution of the electron and ion densities.[5-14] This is primarily due to the fact that kinetic simulations are prohibitively expensive. Even though kinetic models can, in principle, provide detailed information about this phenomenon,[4] fluid models can be readily used to determine their salient features and the effect of changes in external parameters such as gas type, density, and electric field. A problem that arises when using fluid equations is that we must assess what constitutes a proper set of equations for the conditions under investigation. This problem has been extensively treated elsewhere.[15]

In this paper, we present results from numerical simulations of the formation and propagation of streamers in nonattaching (N_2) and attaching (N_2-SF_6 mixture) gases using a one-moment fluid model. Results obtained from this model are compared with those obtained from a kinetic model.[4] In the investigations reported, a pulse of electrons is released from the cathode of a cylindrically symmetric parallel-plate gap. Simultaneously, a voltage pulse (greater than the dc breakdown voltage) is applied to the electrodes. A self-consistent simulation of the evolution of the pulse requires that the fields produced by the space charge generated in the gap be taken into account.

In general, the space charge is characterized by large density gradients and dynamic range. This makes the accurate solution of the moment equations and the determination of the self-consistent field very difficult.[16] A number of approaches have been used to approximate (in more than one dimension) the space-charge distribution, so that the space-charge fields can be readily determined. In these approaches, the "envelope" of the space charge is assumed to be a cylinder either flat-ended or capped by a conical spheroid, hyperboloid, or ellipsoid.[2,14] Inside these envelopes, various models have been chosen for the functional dependence with radius and axial distance of the electron and ion densities (in most cases, the background gas has been nonattaching). Examples of these functional dependences are the constant–net-space-charge–density cylinder (CNC) and the variable–net-space-charge cylinder (VNC).[14] These simplifications lead to space-charge field distributions and consequently particle flows that may give an inaccurate picture of the streamer dynamics. More accurate calculations[4,7,12] and experiments[17-20] show that the radial flow of charge is important in determining the radial density profiles and, consequently, the radial and axial field. Thus, at least, a two-dimensional simulation is necessary.

Less attention has been given to the accurate solution of the fluid equations.[14,21] This presents a different set of problems than solving for the field[22] (the field equation is elliptic, while the fluid equations are hyperbolic). We have developed a numerical algorithm based on flux-corrected transport techniques[23] that allows the solution of these equations in the presence of large gradients and dynamic range.[16] We have used this code, together with a two-dimensional Poisson code,[22] to simulate the evolution of the initial pulse. The simulation is fully two-dimensional. The effects of cathode photoemission, gas photoionization, and electron attachment have been included.

In Sec. II, the simulation model is discussed. The results are presented in Sec. III, and concluding remarks are given in Sec. IV.

II. THE SIMULATION MODEL

A. Model equations

A single-moment equation (the density equation) has been used to describe each of the charged species in the interelectrode volume. The presence of photoionization and/or attachment moderates the density gradients and, consequently, the amplitude of the space-charge field (see Sec. III). Moreover, runaway electrons (which would have to be treated separately) are not observed if the total field at the head of the avalanche is below 1500 Td.[4,24] For these conditions, the single-moment equation is satisfactory in describing the salient features of the dynamics of the charged particles. The evolution of the system is assumed to be cylindrically symmetric, i.e., in (r,z) space.

The dynamical equations are,[6] for electrons,

$$\frac{\partial N_e}{\partial t}+\nabla\cdot N_e\mathbf{V}_e=\alpha N_e\,|\mathbf{V}_e|-\eta N_e\,|\mathbf{V}_e|+S_p\ , \tag{1}$$

and for ions,

$$\frac{\partial N_p}{\partial t}=\alpha N_e\,|\mathbf{V}_e|+S_p\ , \tag{2}$$

$$\frac{\partial N_n}{\partial t}=\eta N_e\,|\mathbf{V}_e|\ , \tag{3}$$

where N_e is the electron density, N_p is the positive-ion density, N_n is the negative-ion density, $\mathbf{V}_e$ is the electron drift velocity, α is the electron-impact ionization coefficient, η is the electron attachment coefficient, and S_p is the source of electron-ion pairs due to photoionization. Drift and diffusion of the ion species have been neglected for the time scale of interest. When the momentum and energy relaxation times and distances are small, we can use the following equation for the electron fluid velocity:

$$N_e\mathbf{V}_e=-\overleftrightarrow{\mathbf{D}}_e\cdot\nabla_e N_e-\mu_e N_e(\mathbf{E}_{\mathrm{sp}}+\mathbf{E}_a)\ , \tag{4}$$

where $\overleftrightarrow{\mathbf{D}}_e$ is the diffusion tensor for electrons, which has a longitudinal and transverse component (D_L,D_T), μ_e is the electron mobility, $\mathbf{E}_a$ is the applied field, and $\mathbf{E}_{\mathrm{sp}}$ is the space-charge field. The values that have been used for the transport parameters and rate coefficients in Eqs. (1)–(4) are given in the Appendix. The numerical method for obtaining a solution to Eq. (1) is described elsewhere.[16]

The space-charge field $\mathbf{E}_{\mathrm{sp}}$ follows from the solution of the Poisson equation

$$\nabla\cdot\mathbf{E}_{\mathrm{sp}}=\frac{q}{\epsilon}(N_p-N_e-N_n)\ , \tag{5}$$

where q is the elementary charge and ϵ is the dielectric constant of the gas. Equation (5) has been solved within the discharge volume (including electrode boundaries) using the two-dimensional (2D) method of Kunhardt and Williams.[22] Equations (1)–(5) are the set of equations that describes the evolution of the system. Photoionization, electron attachment, and photoemission from the electrodes are also considered in the model.

B. Production of photoelectrons in the gas and at the cathode

Photoionization of the gas by radiation produced by the avalanche is taken into account in Eq. (1) via the term S_p. The photoionization data of Penny and Hummert[25] have been taken as a model for the process. To properly utilize these data, the special geometry of their experiment needs to be considered.[7,9] The source of photoionizing radiation is assumed to be a ring at (r_2,z_2). This radiation is absorbed in a ring at (r_1,z_1) and generates dN_{ph} photoelectrons, given by the expression,

$$dN_{\mathrm{ph}}(r_1,r_2,|z_1-z_2|)=\alpha(r_2,z_2)N_e(r_2,z_2)2\pi r_2\,dr_2\,dz_2 \times g(r_1,r_2,|z_1-z_2|)p\ , \tag{6}$$

where p is the background gas pressure,

$$g(r_1,r_2,|z_1-z_2|)=\int_0^{\pi}\psi(rp)A(r_1,r_2,|z_1-z_2|,\phi) \times S(r_1,r_2,|z_1-z_2|,\phi)d\phi\ . \tag{7}$$

ψ is the photoionization rate,[25] and

$$r=[(z_1-z_2)^2+r_1^2+r_2^2-2r_1r_2\cos\phi]^{1/2}\ . \tag{8}$$

ϕ is the angle between the two points in a plane perpendicular to z. In this expression, the thickness S and effective area A of a volume element depend on r_1, r_2, and $|z_1-z_2|$; that is, on the axial distance between source and target, and on the angle ϕ. The total number of photoelectrons generated in the ring (r_1,z_1) is obtained from Eq. (6) by integrating over all (r_2,z_2) sources,

$$N_{\mathrm{ph}}(r_1,z_1)=\int_0^d\int_0^\infty dN_{\mathrm{ph}}(r_1,r_2,|z_1-z_2|)\ , \tag{9}$$

where d is the gap separation.

Photoemission from the cathode has been treated as follows. The density of the excited molecules $N_{\mathrm{ex}}(r_1,z)$ is given by

$$N_{\mathrm{ex}}(r_1,z)=\delta N_e(r_1,z)\ , \tag{10}$$

where δ is the excitation coefficient (see Appendix). The photon flux F per unit area at the cathode is

$$F(r)=\int_0^d\int_0^\infty N_{\mathrm{ex}}(r',z')g_1(r',z',r)r'\,dr'\,dz'\ , \tag{11}$$

where

$$g_1(r',z',r)=\int_0^{2\pi}d\phi\frac{z'}{R^3}e^{-\mu_a R}\ , \tag{12}$$

d is the gap separation, $R=(z'^2+r^2+r'^2-2rr'\cos\phi)^{1/2}$, and μ_a is the absorption coefficient (see Appendix). The total number of electrons N_{ec} generated at the cathode is

$$N_{ec}=F(r)2\pi r\Gamma_c\,dr\ .$$

For the cathode efficiency Γ_c, a value of 4×10^{-3} has been assumed in accordance with Ref. 7.

III. RESULTS AND DISCUSSION

The results presented in this paper are from simulations of a cylindrically symmetric parallel-plate system with infinite radius. The distance between the electrodes is 0.5 cm, and the gas density is 2.45×10^{19} cm^{-3} for N_2 and a 30% SF_6–70% N_2 mixture. The initial distribution of charge is chosen to simulate the problem of avalanche development from a single electron (no ions) located in front of the cathode.[4] The initial electron-density distribution is

$$N_e(r,z)=5\times10^4\exp\left[-\left[\frac{r}{1.945\times10^{-2}}\right]^2\right]\times\exp\left[-\left[\frac{z-2.925\times10^{-2}}{1.95\times10^{-2}}\right]^2\right]\ \text{cm}^{-3},$$

where the (r,z) extent is limited to a few cells and the unit of r and z is centimeters. The results for N_2 are presented first, followed by those for the SF_6-N_2 mixture. This mixture is taken as representative of a strongly attaching gas.

A. Nitrogen

Unless stated otherwise, the results presented are for an applied field to density ratio of $E_a/N=241$ Td ($E/p=78.1$ V/cm Torr, which corresponds to 68% overvoltage at a density of 2.45×10^{19} cm^{-3}). Calculated contours of constant densities in r-z space are shown in Fig. 1 at times 7.2 nsec [Fig. 1(a)], 8.5 nsec [Fig. 1(b)], 9.1 nsec [Fig. 1(c)], and 9.2 nsec [Fig. 1(d)] after the start of the initial pulse. The early phases of the avalanche are not shown. For these experimental conditions, the electron avalanche becomes "critical"[26] at $t\simeq6$ nsec, at the "critical" distance $z_{\text{cr}}\simeq0.14$ cm [see Fig. 1(a)]. Nearly at the same time, streamer fronts appear and propagate toward the anode and the cathode [see Fig. 1(b)]. The velocity along the z direction of the charge-density fronts as a function of time is shown in Fig. 2. An increase in the front velocity is observed upon formation of the streamer fronts. This is clearly seen for the anode-directed front (Fig. 3). As the anode-directed streamer progresses, its velocity becomes nearly constant, until it is affected by electrode processes (image charges, in this case). The field enhancement created by image charges causes a second increase in the front velocity (Fig. 3). The cathode-directed streamer forms close to the cathode, with the result that electrode processes (secondary emission and image charges) cause a continuous increase in the velocity of the front. The behavior of streamer fronts as a function of time, described above, has been observed in a number of investigations.[6–8]

As previously mentioned, as the cathode-directed streamer approaches the electrode [at $\simeq8.5$ nsec, Fig. 1(b)], the field at the front is further enhanced by the image charges (Fig. 3). If the avalanche becomes critical near the cathode [as is the case in Fig. 1(b)], the image field also influences the anode front, and the radial field increases rapidly away from $r=0$. Thus the total field for $r\gtrsim0$ has a strong radial component and, in fact, it can become larger than the field at $r=0$. This causes the density off axis for the anode-directed streamer to be higher than that on axis. This behavior has also been observed in Monte Carlo simulations.[4] At $t=9.11$ nsec, the cathode-directed streamer reaches the cathode, and the field is redistributed. The anode front has moved sufficiently far from the cathode by this time that the density on axis is again at maximum. It would be interesting to see how this effect influences the development in three dimensions.

In the later stages of development, a radial constriction of the electron-density contour is observed[8] [see Figs. 1(c) and 1(d) for $N_e\simeq10^{13}$ cm^{-3}]. This behavior is caused by the ion space charge left inside the streamer which accelerates electrons produced at $r\neq0$ towards the center. This results in a radially directed inward flow of electrons. At $\simeq9.19$ nsec, the anode-directed streamer reaches the anode [see Fig. 1(d)]. Shortly after both streamers reach the electrodes, an ionized channel exists between the anode and cathode, which has a radius of approximately 0.02 cm. The mean resistance of this channel has been calculated to be $\simeq74$ kΩ. In all cases investigated in N_2, the channel resistance is of this order of magnitude. The subsequent evolution of this channel leads to the breakdown of the insulating properties of the gap.

The effect of delayed cathode photoemission (due to the lifetime τ of the excited state producing the radiation) on the propagation of the cathode-directed streamer is shown in Fig. 4. In those simulations, $E_a/N=432$ Td ($E_a/p=140$ V/cm Torr, which corresponds to 200% overvoltage). This streamer develops very early and reaches the cathode at $t\sim1$ nsec. As τ decreases, the secondary avalanches that develop from the cathode become larger. This causes a radial expansion of the ionized channel; however, it does not affect the propagation of the anode-directed streamer. From Fig. 4, the secondary avalanches are seen to have a much lower density than the primary channel. Because of this, it is difficult to experimentally obtain the profiles shown in Fig. 4, and thus determine, by comparison, the effective τ of the radiation produced by the channel.

We have also investigated the effect of the radial extent of the initial charge distribution on the formation and propagation of streamers. For the density contours shown in Fig. 5, the initial distribution of electrons is a disk with radius 0.3 cm and thickness 0.1 cm. The integrated total number of electrons in this disk is 6000 and $E_a/N=432$ Td. τ has been taken to be 0.1 nsec. As in the previous case, the positive space charge inside the region with higher ionization accelerates electrons towards the center. The returning ionizing wave (see shaded region in Fig. 5) from the cathode, and the constriction of the anode-directed streamer, eventually come together, and continue as a filamentary front. A similar behavior has been observed by Koppitz (Fig. 1, Ref. 27) and Stritzke *et al.* (Fig. 5, Ref. 28).

The propagation speed of the anode-directed streamer is a function of the diameter of the space-charge distribution. We have found that the speed increases with diameter. This is due to the fact that the radial flow at the front, near the axis, decreases with increasing diameter.

The velocity of the anode-directed streamer versus E/p, for a filamentary space-charge distribution, is shown in Fig. 6. These results have been obtained for $p=1$ atm. In this pressure range, there are few experimental data. Chalmers *et al.*[29] have conducted experiments with filamentary distributions at 300 Torr in N_2, and have observed a propagation velocity of 6×10^7 cm/sec at 25% overvoltage. In view of these experiments, our results are reasonable. Koppitz[27] has presented results for wide space-charge distributions at 300 Torr in N_2. For 20% overvoltage, he has reported a streamer of 1.4×10^8 cm/sec. This is consistent with our observation of the increase in streamer velocity.

To assess the validity of a single-moment description of the development of a streamer under the conditions investigated, we have compared the results with those obtained using a kinetic simulation[4] (using Monte Carlo methods). The kinetic results are for $E_a/N=300$ Td (128% overvoltage), whereas the moment results are for $E_a/N=263$ Td (100% overvoltage) (Fig. 7). The initial conditions for both are nearly the same (i.e., "single-electron initiation"). The contours of constant density in both cases are very close, although the kinetic results are displaced slightly ahead (since the E/N is higher). From these contours, the streamer velocity for the kinetic and moment models has been found to be 1.4×10^8 and 1.0×10^8 cm/sec, respectively. In the presence of photoionization, we have found that for the conditions investigated, the single-moment model gives reasonable results. However, we expect that this model will no longer be adequate in situations where the photoionization yield is low and, consequently, the gradients become large. This is presently under investigation.

B. Electronegative gas: 30% SF_6–70% N_2

The results presented are for an applied field to density ratio E_a/N equal to 282 Td ($E/p=93.9$ V/cm Torr) at a gas density N equal to 2.45×10^{19} cm^{-3}. The development of the contours of constant electron density and

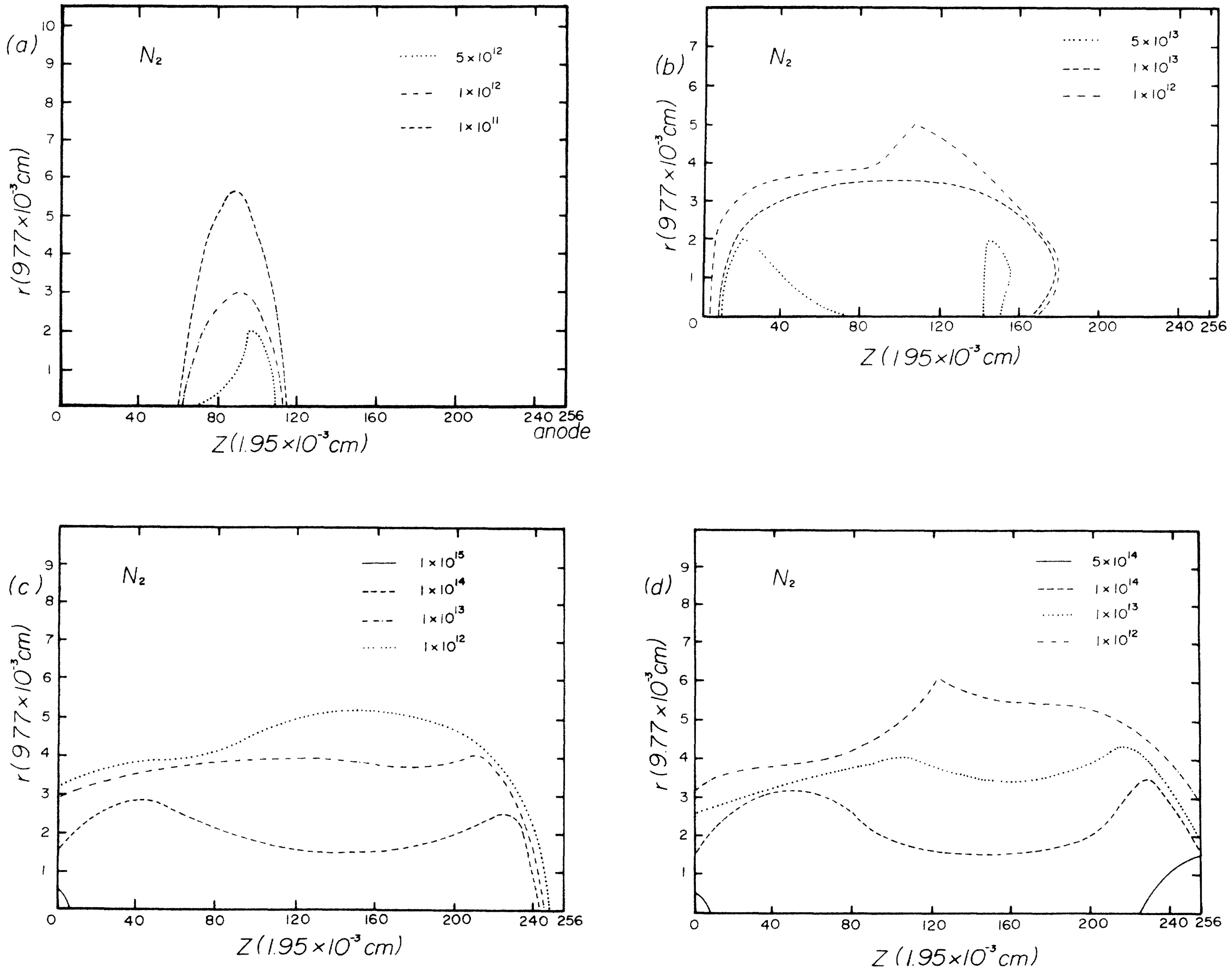

FIG. 1. Evolutions of constant electron-density contours in r-z space, for $E_a/N=234$ Td and $N=2.45\times10^{19}$ cm^{-3} in N_2. (a)–(d) correspond to $t=7.2$, 8.5, 9.1, and 9.2 nsec, respectively. The grid sizes are $\Delta r=9.77\times10^{-3}$ cm and $\Delta z=1.95\times10^{-3}$ cm. The anode is located at $z=256\ \Delta z$. The unit of the density contours is cm^{-3}.

longitudinal field on axis is shown in Figs. 8 and 9, respectively. Near $t \simeq 7.69$ nsec space-charge effects become important. At this time, the center of the space-charge distribution is at $z_{\text{cr}} = 1.9$ cm. The anode-directed streamer appears, and subsequently ($t \sim 8.49$ nsec), the electron density just inside the streamer front decreases because of attachment. In this region, $\alpha - \eta = \bar{\alpha} < 0$. At $t \sim 9.29$ nsec, the cathode-directed streamer appears, and a similar decrease in density is observed just inside the front. Note that the cathode-directed streamer appears much later, relative to the anode-directed streamer, than when it appears for N_2.

As the streamer progresses, spatial oscillations are observed in the electron-density profile (see curve for $t \sim 10.44$ nsec, Fig. 8). This phenomenon can be explained using the qualitative profiles shown in Fig. 10. Since the electron mobility is higher than that of either positive or negative ions, the ions are stationary in the time scales of interest. Thus in a time Δt, the electron population is displaced from the ion population as shown in Fig. 10(a). The resulting total axial field is shown in Fig. 10(c). In an electronegative gas, the critical field E_c is defined by the condition that the net electron production is zero. This occurs when $\alpha = \eta$ or $\bar{\alpha} = 0$.[30] For $\bar{\alpha} < 0$, or $E < E_c$, the electron density decreases (with a concomitant increase in the negative-ion density) due to electron attachment by SF_6. From Fig. 10, we observe that there are two attachment regions ($E < E_c$), where the electron density decreases. In the other regions, where $\bar{\alpha} > 0$, or $E > E_c$, the electron density increases. Note that $\bar{\alpha}$ is a very sensitive function of E. At $t + 2\Delta t$, the density profile exhibits an oscillation in space. As the streamers propagate, so that the fronts move away from each other, the field inside the space-charge region increases and becomes greater than E_c, and ionization starts again. This process causes the spatial oscillations observed in Fig. 8. This is not observed in N_2.

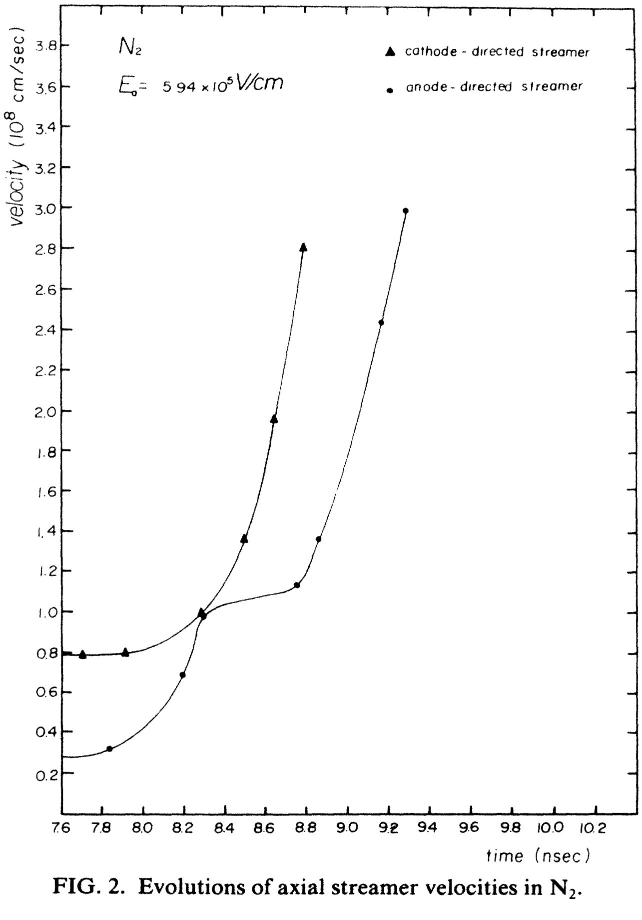

FIG. 2. Evolutions of axial streamer velocities in N_2.

The spatial oscillations have also been observed by Morrow[11] in one-and-one-half-dimensional ($1\frac{1}{2}$D) calculations in SF_6. Our results in N_2-SF_6 have features similar to those obtained by him in SF_6.[11] These oscillations, however, have not been observed in other attaching gases.[6,11] In the investigations in air by Kline,[6] the attachment rate η is taken as a constant, so that it is difficult to see the attachment effect due to the streamer space-charge field. In the point-to-plane investigations in oxygen by Morrow,[11] the nonuniform field caused by the tip dominates the phenomenon. In our case, as in Morrow's[11] a negative-ion region develops due to attachement in the region just inside the streamer front. However, unlike the point-to-plane geometry, in the parallel-plate geometry, as the streamer fronts move apart, the field inside the space-charge distribution increases above E_c. As discussed above, this causes the increase in the electron density and the spatial oscillations observed. These spatial oscillations may be the cause of the discontinuities in the bright regions of SF_6 discharges experimentally observed by Pfeiffer and co-workers.[18,19,31] The anode-directed streamer velocity that they have measured, in an 8-mm gap with SF_6 at 2 bar and an applied voltage of 140 kV, is 2×10^8 cm/sec. In these experiments, the applied field is nonuniform, so that it is difficult to determine the value of the external field at the location of the streamer. From our calculation, the field that corresponds to this streamer velocity is $E = 70$ kV/cm (Fig. 11). This value of E in the gap is reasonable. Further analysis under uniform field conditions is necessary.

A fixed radius simulation has been carried out by Wiegart *et al.*[32] for $E = 92$ kV/cm. The total field distribution they have calculated agrees well (qualitatively) with our results. This is also true of the anode-directed streamer velocity. The increase in streamer velocity with diameter of the space-charge distribution has also been observed by them.

At $t \sim 11.40$ and ~ 11.54 nsec (Fig. 8), the anode- and cathode-directed streamers reach the respective electrodes. The returning ionizing waves are subsequently observed. When the streamers reach the electrode, the field in the gap is almost equal to the applied field. This is because the conductivity of the ionized channel is very low. Breakdown occurs when this conductivity increases due to channel heating. For these conditions, the ionized channel has a radius of approximately 0.02 cm and a mean resistance of 500 kΩ.

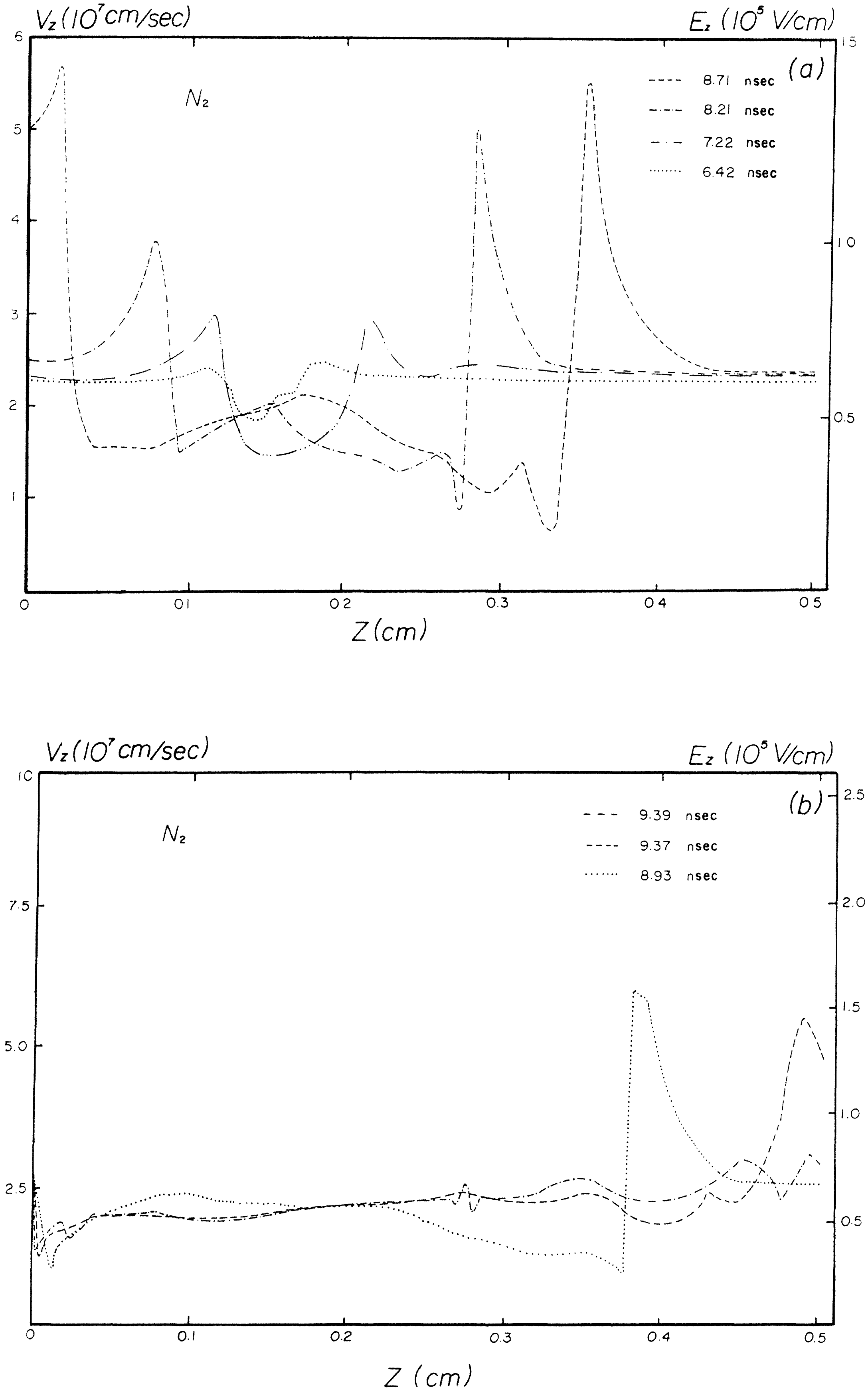

FIG. 3. Evolution of longitudinal field (or drift velocity) on axis in N_2.

IV. CONCLUDING REMARKS

In this paper, results from 2D simulations of the development and propagation of streamers in nonattaching (N_2) and attaching (SF_6-N_2) gases have been presented. Significant differences have been observed in the density and field profiles of these two types of gases. The cathode-directed streamer in SF_6-N_2 mixtures appears at a later time relative to the anode-directed streamer than when it appears for N_2. Because of the existence of an attaching region ($E < E_c$) close to the streamer front in attaching gases, less space-charge separation occurs at the front of the streamers than what occurs in nonattaching gases. This has the effect that the magnitude and slope of the axial space-charge field is smaller in attaching gases than in nonattaching gases (see Figs. 3 and 9).

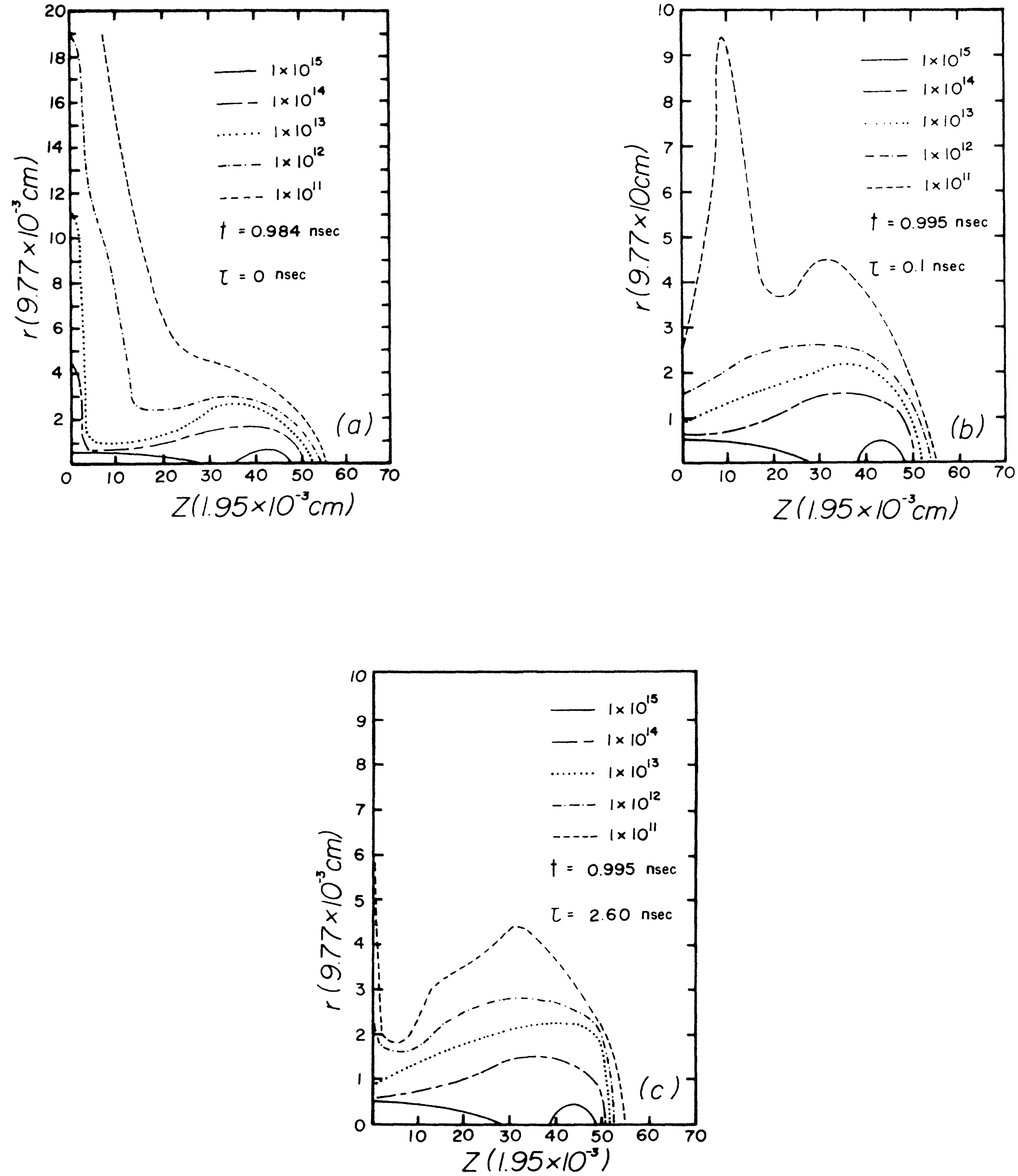

FIG. 4. Constant electron-density contours in r-z space for different delay τ of the photoemitted electrons. (a)–(c) correspond to $\tau=0$, 0.1, and 2.6 nsec, respectively. $E_a/N=418$ Td and $N=2.45\times10^{19}$ cm^{-3} in N_2. The grid sizes are the same as those of Fig. 1. The unit of the density contours is cm^{-3}.

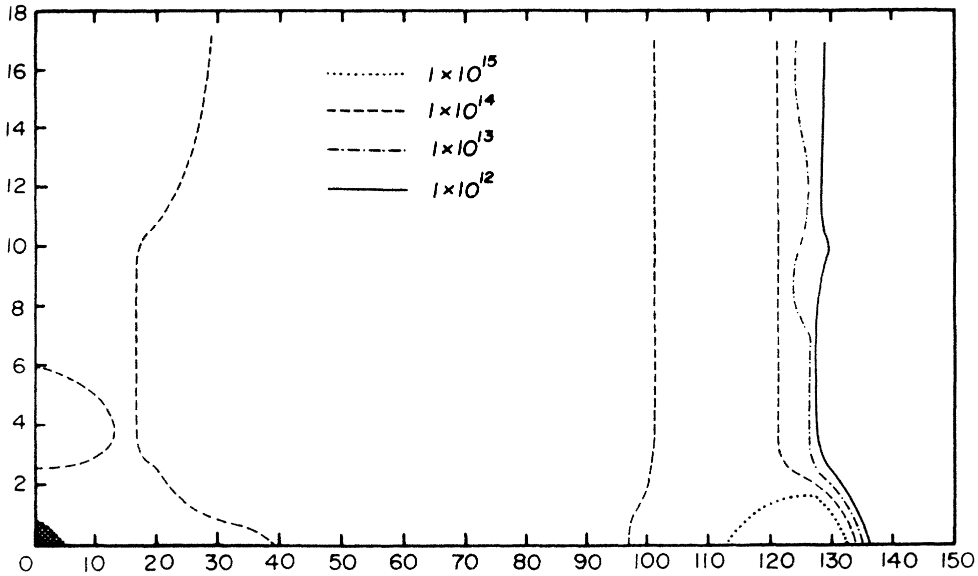

FIG. 5. Constant electron-density contours in r-z space at $t=0.787$ nsec, for $E_a/N=418$ Td, $N=2.45\times10^{19}$ cm^{-3}, and $\tau=0.1$ nsec, in N$_2$. The unit of the density contours is cm^{-3}. The initial distribution of electrons is a disk with radius 0.3 cm and thickness 0.1 cm. The total number of electrons in this disk is 6000. The grid sizes are the same as those in Fig. 1.

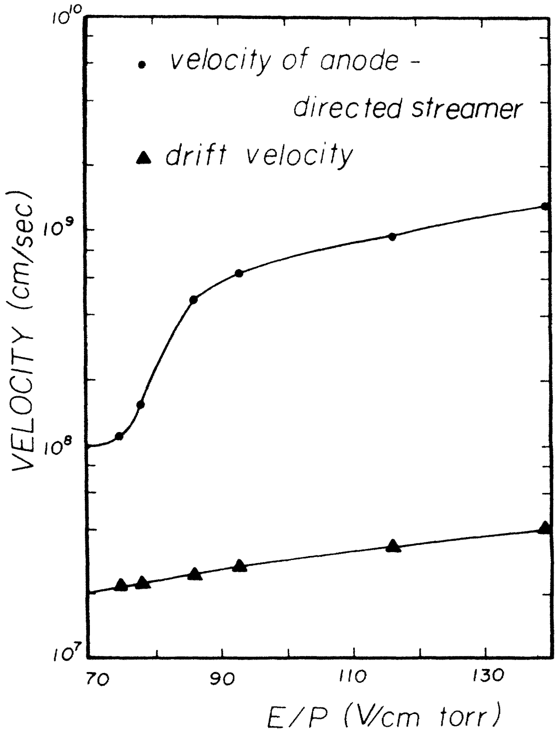

FIG. 6. Velocity of anode-directed streamer vs E/p in N$_2$. The breakdown field is 35.4 kV/cm and the corresponding $E/p=46.5$ V/cm Torr ($E/N=139.5$ Td).

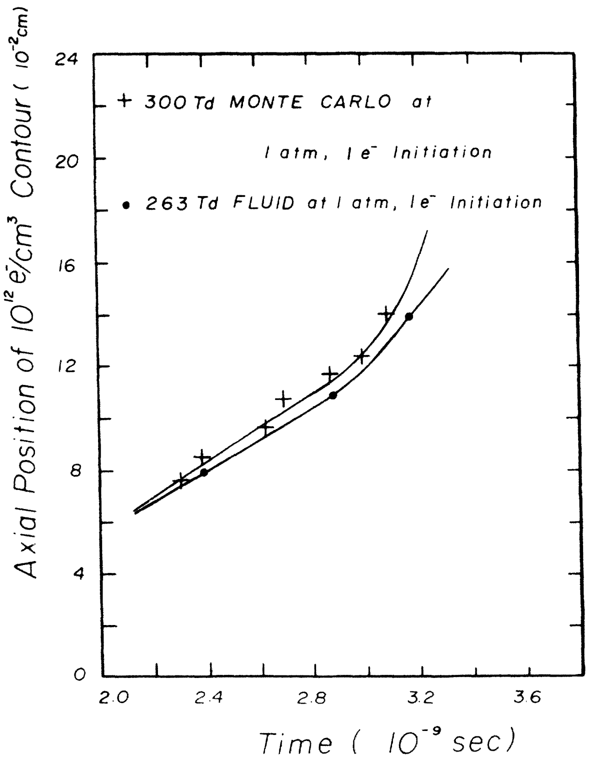

FIG. 7. Axial position as a function of time of 10^{12} cm^{-3} density contour obtained with fluid and kinetic models. The interval shown corresponds to the avalanche to streamer transition stage.

The N_2, at the time of streamer formation, the field inside the space-charge region is not zero, but slightly greater than the field for which $\alpha \simeq 0$. This has previously been observed in Monte Carlo simulations.[4] As the streamer fronts move apart, the field inside the ionized region increases, until it becomes almost equal to the applied field when the streamers reach the electrodes. The resulting weakly ionized channel has a radius in the range of 10^{-2} cm and a resistance in the 10^5-ohm range. In SF_6-N_2 mixtures, in addition to the above observations, the electron density has been observed to exhibit spatial oscillations.

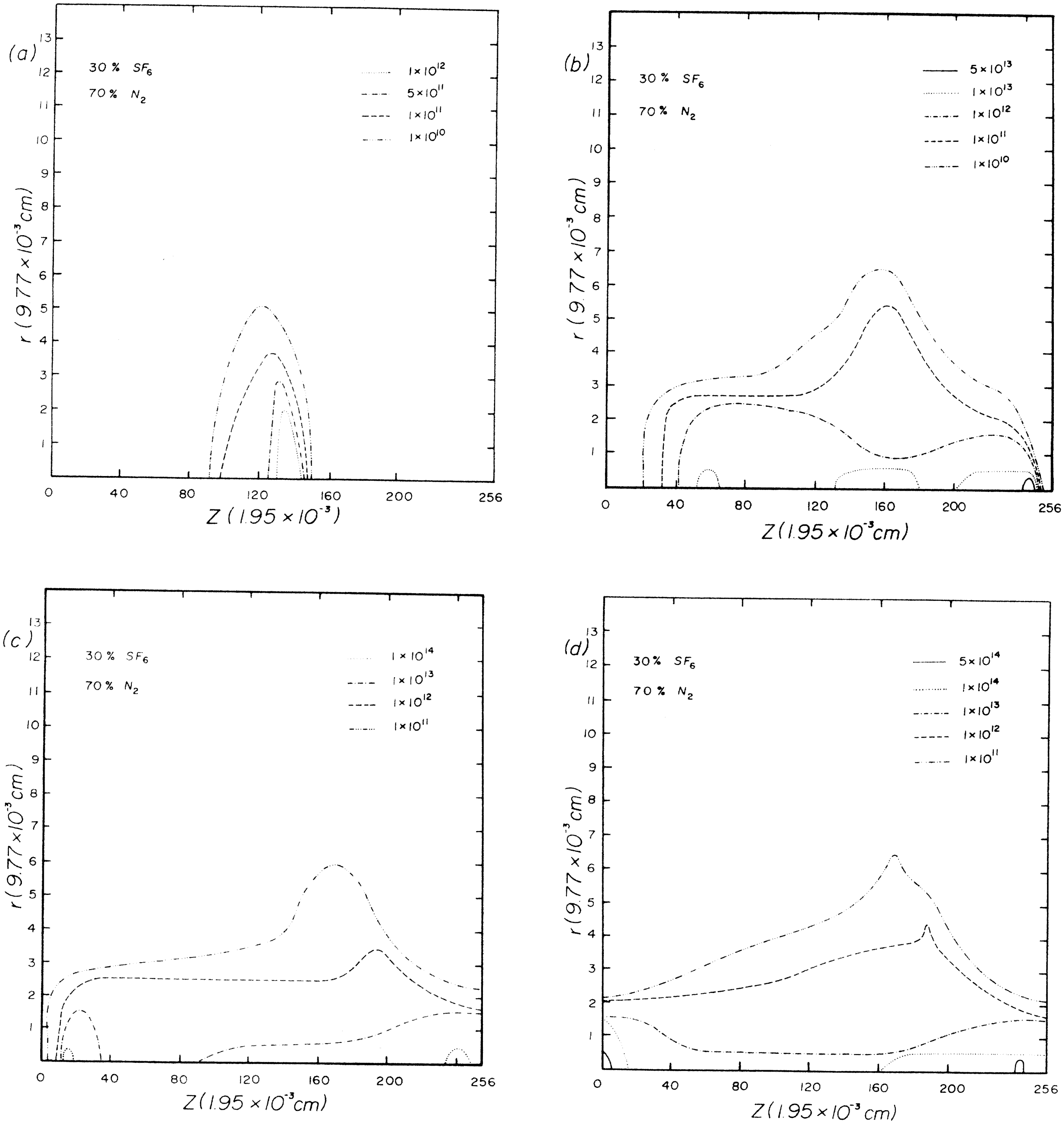

FIG. 8. Evolution of constant electron-density contours in r-z space for $E_a/N = 282$ Td and $N = 2.45 \times 10^{19}$ cm^{-3} in the SF_6-N_2 mixture. (a)–(d) correspond to $t = 8.49$, 10.44, 11.4, and 11.54 nsec, respectively. The grid sizes and the anode location are the same as those of Fig. 1.

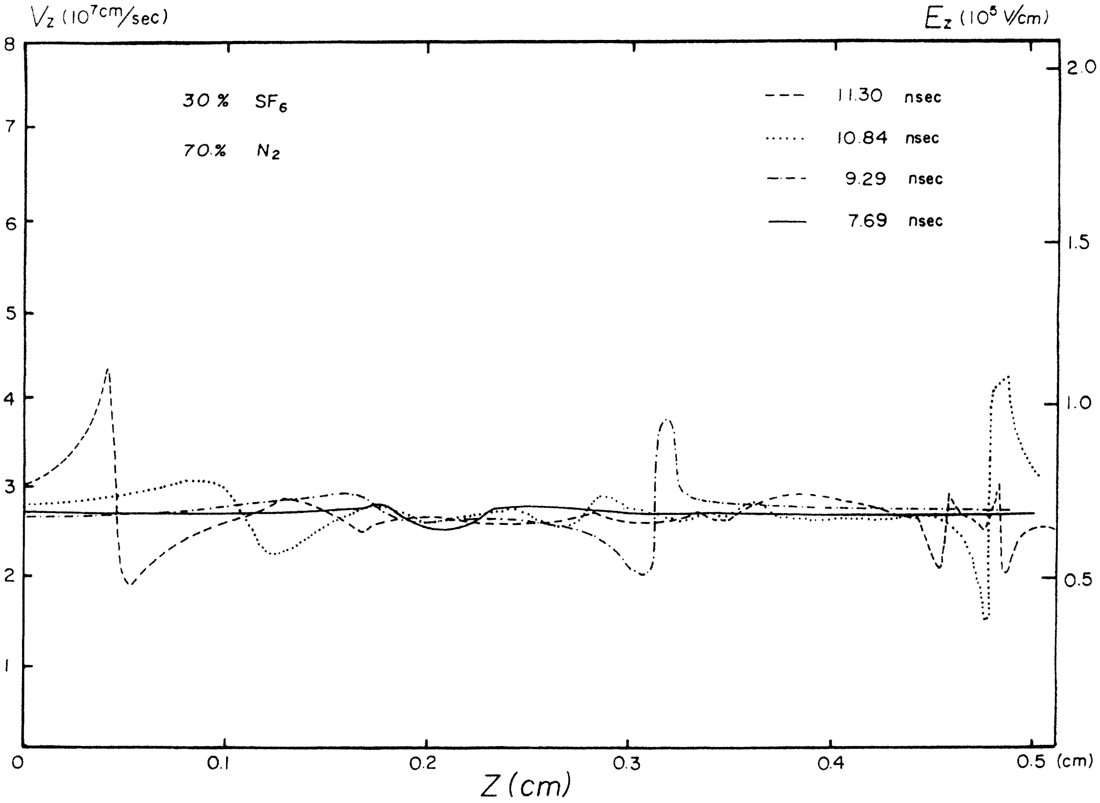

FIG. 9. Evolution of the longitudinal electric field on axis in the SF_6-N_2 mixture.

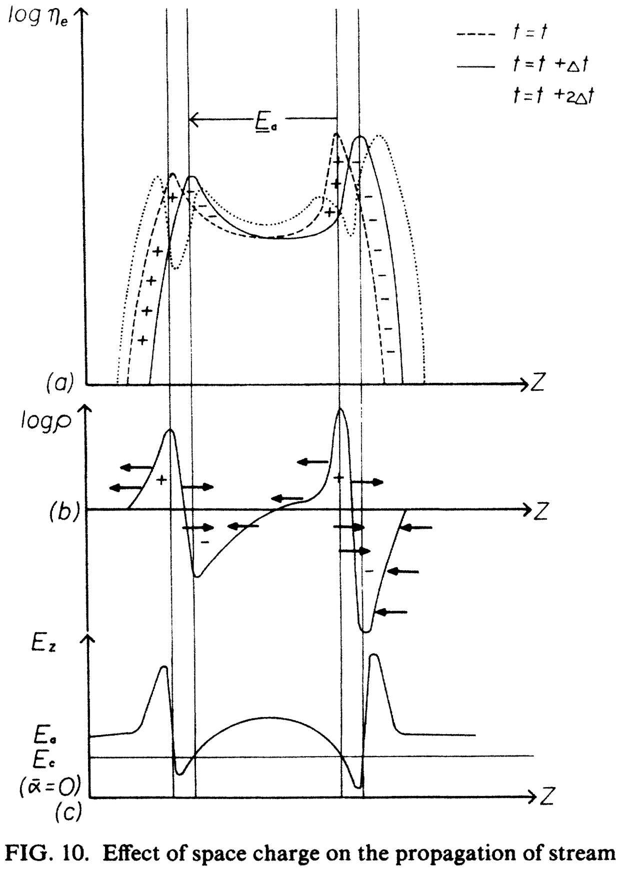

FIG. 10. Effect of space charge on the propagation of streamers in the N_2-SF_6 mixture. E_a is the applied field and E_c is the critical field.

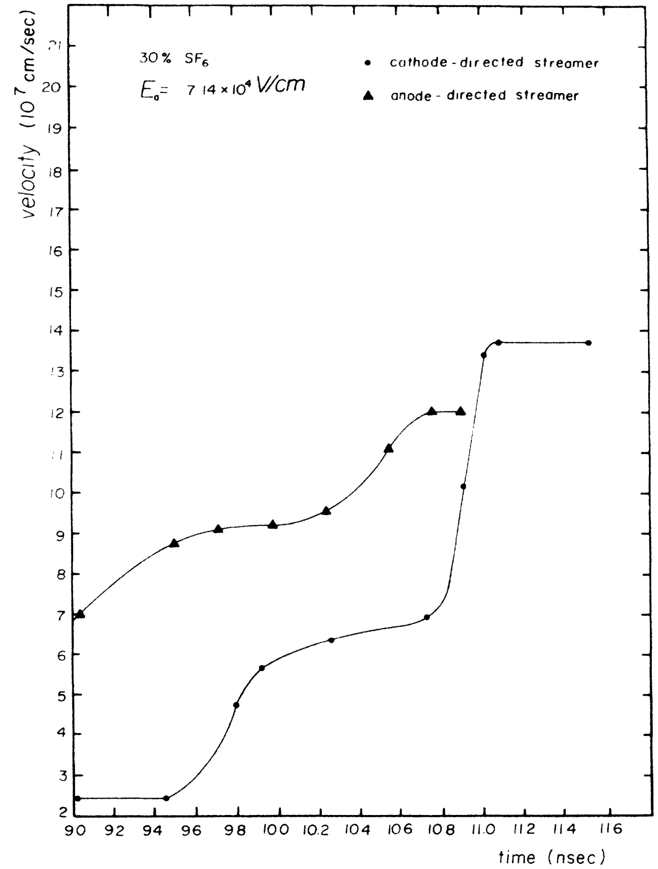

FIG. 11. Evolutions of the longitudinal velocity of streamers in the SF_6-N_2 mixture.

ACKNOWLEDGMENT

This work has been supported by the U.S. Office of Naval Research (ONR).

APPENDIX: INPUT DATA FOR SIMULATION

For α,

$$\alpha/p = 5.7\exp(-260P/E)\ \text{Torr}^{-1}\,\text{cm}^{-1}$$

for N_2[6];

$$\alpha = 25\,316\exp(-385P/E)\ \text{cm}^{-1}$$

for 30% SF_6–70% N_2 mixture at a total pressure of 760 Torr.[33]

For η,

$$\eta = 1700\exp(-0.017\,88E/p)$$

for 30% SF_6–70% N_2 mixture at a total pressure of 760 Torr.[33]

For D,

$$D_L\ (\text{longitudinal}) = 1800\ \text{cm}^2\,\text{sec}^{-1}\,,$$

$$D_T\ (\text{transverse}) = 2190\ \text{cm}^2\,\text{sec}^{-1}$$

at 760 Torr and room temperature.[34]

For μ,

$$\mu_e = 2.9\times 10^5/p\ \text{cm}^2\,\text{V}^{-1}\,\text{sec}^{-1}$$

for N_2;[9]

$$\mu_e = 2.8933\times 10^5/p\ \text{cm}^2\,\text{V}^{-1}\,\text{sec}^{-1}$$

for 30% SF_6–70% N_2 mixture;[33] δ_0 is the excitation coefficient for $C^3\Pi_u$ without quenching:[35]

$$\frac{\delta_0}{\alpha} = 0.101 + \frac{268}{(E/p)} - \frac{353.4\times 10^2}{(E/p)^2} + \frac{547.3\times 10^4}{(E/p)^3} - \frac{160.5\times 10^6}{(E/p)^4} + \frac{2.24\times 10^7}{(E/p)^5}\,.$$

The excitation coefficient δ at pressure p is

$$\frac{\delta}{\alpha} = \frac{\alpha_0}{\alpha(1+p/p_q)}\,,$$

where p_q (which equals 60 Torr) is the quenching pressure of $C^3\Pi_u$.[36] The absorption coefficient μ_a of $C^3\Pi_u$ is $1.2\times 10^{-3}\ \text{cm}^{-1}\,\text{Torr.}^{-1}$

---

[1] E. E. Kunhardt, in *Proceedings of the XVII International Conference on Phenomena in Ionized Gases, Budapest, 1985,* edited by J. S. Bakos and Z. Sorlei (KFKI, Budapest, 1985), p. 345.

[2] E. D. Lozanskii, Usp. Fiz. Nauk. **120**, 363 (1976) [Sov. Phys.—Usp. **19**, 894 (1976)].

[3] L. E. Kline and J. Siambis, Phys. Rev. A **5**, 794 (1972).

[4] E. E. Kunhardt and Y. Tzeng, in *Proceedings of the IV International Symposium on Gaseous Dielectrics,* edited by L. G. Christophorou (Plenum, New York, 1984), p. 146.

[5] A. L. Ward, J. Appl. Phys. **36**, 2540 (1965).

[6] L. E. Kline, J. Appl. Phys. **45**, 2046 (1974); **46**, 1994 (1975).

[7] K. Yoshida and H. Tagashira, J. Phys. D **9**, 485 (1976); **9**, 491 (1976).

[8] K. Yoshida, T. Taniguchi, and H. Tagashira, J. Phys. D **12**, L3 (1976).

[9] A. J. Davies, C. J. Evans, P. Townsend, and P. M. Woodison, Proc. IEE **124**, 179 (1977).

[10] W. Reininghaus, J. Phys. D **40**, 1593 (1973).

[11] R. Morrow, Phys. Rev. A **32**, 1799 (1985); **35**, 1778 (1987).

[12] S. Dhali and P. F. Williams, Phys. Rev. A **31**, 1219 (1985).

[13] I. M. Bortnik, I. I. Kochetov, and K. N. Ul'yanov, Teplofiz. Vys. Temp. **20**, 193 (1982).

[14] P. Bayle and B. Cornebois, Phys. Rev. A **31**, 1046 (1985).

[15] E. E. Kunhardt, J. Wu, and B. Penetrante, Phys. Rev. A **37**, 1654 (1988).

[16] E. E. Kunhardt and J. Wu, J. Comput. Phys. **68**, 127 (1987).

[17] K. H. Wagner, Z. Phys. **189**, 465 (1966); **204**, 177 (1967).

[18] W. Pfeiffer and W. Schmitz, in Third International Symposium on High Voltage Engineering, Milan, 1979 (unpublished), p. 31.01.

[19] W. Pfeiffer, A. Leitl, P. Völker, and H. Fischer, Appl. Opt. **20**, 10 (1981).

[20] M. C. Cavenor, Aust. J. Phys. **22**, 155 (1969).

[21] R. Morrow, J. Comput. Phys. **43**, 1 (1981).

[22] E. E. Kunhardt and P. F. Williams, J. Comput. Phys. **57**, 403 (1985).

[23] J. Zalesake, J. Comput. Phys. **31**, 335 (1979).

[24] Y. Tzeng and E. E. Kunhardt, Phys. Rev. A **34**, 2148 (1986).

[25] G. W. Penny and G. T. Hummert, J. Appl. Phys. **41**, 572 (1970).

[26] H. Raether, *Electron Avalanches and Breakdown in Gases* (Butterworths, London, 1964).

[27] J. Koppitz, J. Phys. D **6**, 1494 (1973).

[28] P. Stritzke, I. Sander, and H. Raether, J. Phys. D **10**, 2285 (1977).

[29] I. Chalmers, H. Duffy, and D. Tedford, Proc. R. Soc. London, Ser. A **239**, 171 (1972).

[30] A. Pedersen, IEEE Trans. Power Appar. Syst. **PAS-89**, 2043 (1970).

[31] M. Giesselmann and W. Pfeiffer, in *Proceedings of the IV International Symposium on Gaseous Dielectrics,* edited by L. G. Christophorou (Plenum, New York, 1984), p. 431.

[32] N. Wiegart, F. Pinnekamp, and S. A. Boggs, Canadian Electrical Association Report No. CEA-153-T-310, 1985 (unpublished).

[33] J. P. Novak and M. F. Frechette, J. Appl. Phys. **55**, 107 (1984).

[34] J. Dutton, J. Phys. Chem. Ref. Data **4**, 664 (1975).

[35] S. Badaloni and I. Gallimberti, *Basic Data of Air Discharges* (University of Padova Press, Padova, 1972), p. 73.

[36] W. Legler, Z. Phys. **173**, 169 (1963).